Figure S1

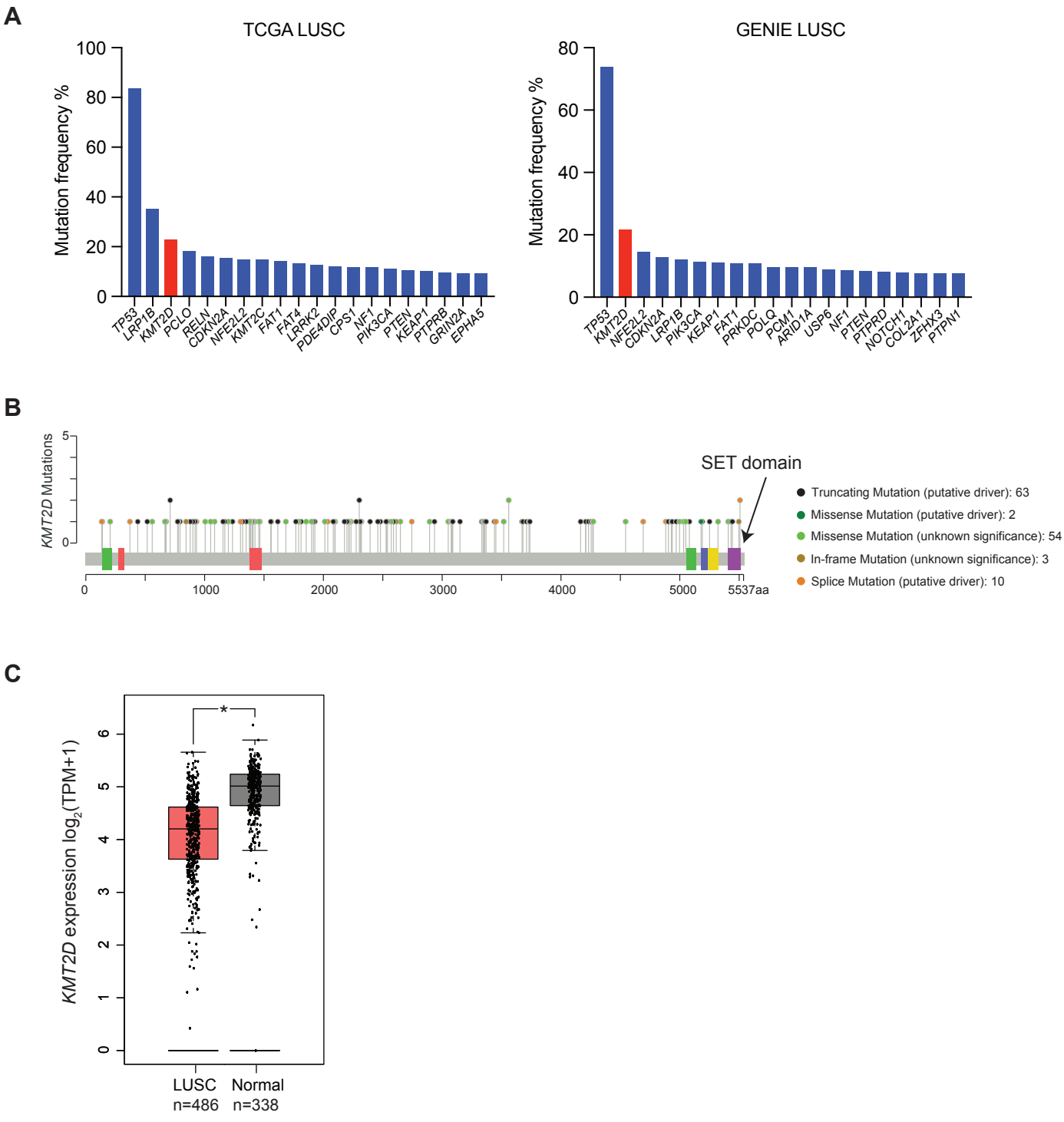
A
TCGA LUSC
Mutation frequency %
100
80
60
40
20
0
TP53
LRP1B
KMT2D
PCLO
RELN
CDKN2A
NFE2L2
KMT2C
FAT1
FAT4
LRRK2
PDE4DIP
CPS1
NF1
PIK3CA
PTEN
KEAP1
PTPRB
GRIN2A
EPHA5
GENIE LUSC
Mutation frequency %
80
60
40
20
0
TP53
KMT2D
NFE2L2
CDKN2A
LRP1B
PIK3CA
KEAP1
FAT1
PRKDC
POLQ
PCM1
ARID1A
USP6
NF1
PTEN
PTPRD
NOTCH1
COL2A1
ZFHX3
PTPN1
B
KMT2D Mutations
5
0
SET domain
0
1000
2000
3000
4000
5000
5537aa
Truncating Mutation (putative driver): 63
Missense Mutation (putative driver): 2
Missense Mutation (unknown significance): 54
In-frame Mutation (unknown significance): 3
Splice Mutation (putative driver): 10
C
KMT2D expression log2(TPM+1)
0
1
2
3
4
5
6
*
LUSC
n=486
Normal
n=338

Figure S1. *KMT2D* is frequently mutated in LUSC, related to Figure 1

(A) Bar graphs showing the frequently mutated tumor-related genes in LUSC according to the TCGA and GENIE databases. *KMT2D* is mutated in 111 of 484 LUSC samples in TCGA PanCancer Atlas dataset and in 301 of 1385 LUSC samples in GENIE dataset.

(B) Lollipop graph showing mutation profiles (truncating, missense, in-frame, and splice) of *KMT2D* gene in the LUSC TCGA PanCancer Atlas dataset (n=469).

(C) Box plot showing *KMT2D* mRNA expression levels in LUSC samples (from TCGA dataset) and normal lung tissues (from TCGA and GTEx projects). The plot was generated using the GEPIA2 online server (http://gepia2.cancer-pku.cn/). *$p < 0.05$ (ANOVA).

Figure S2

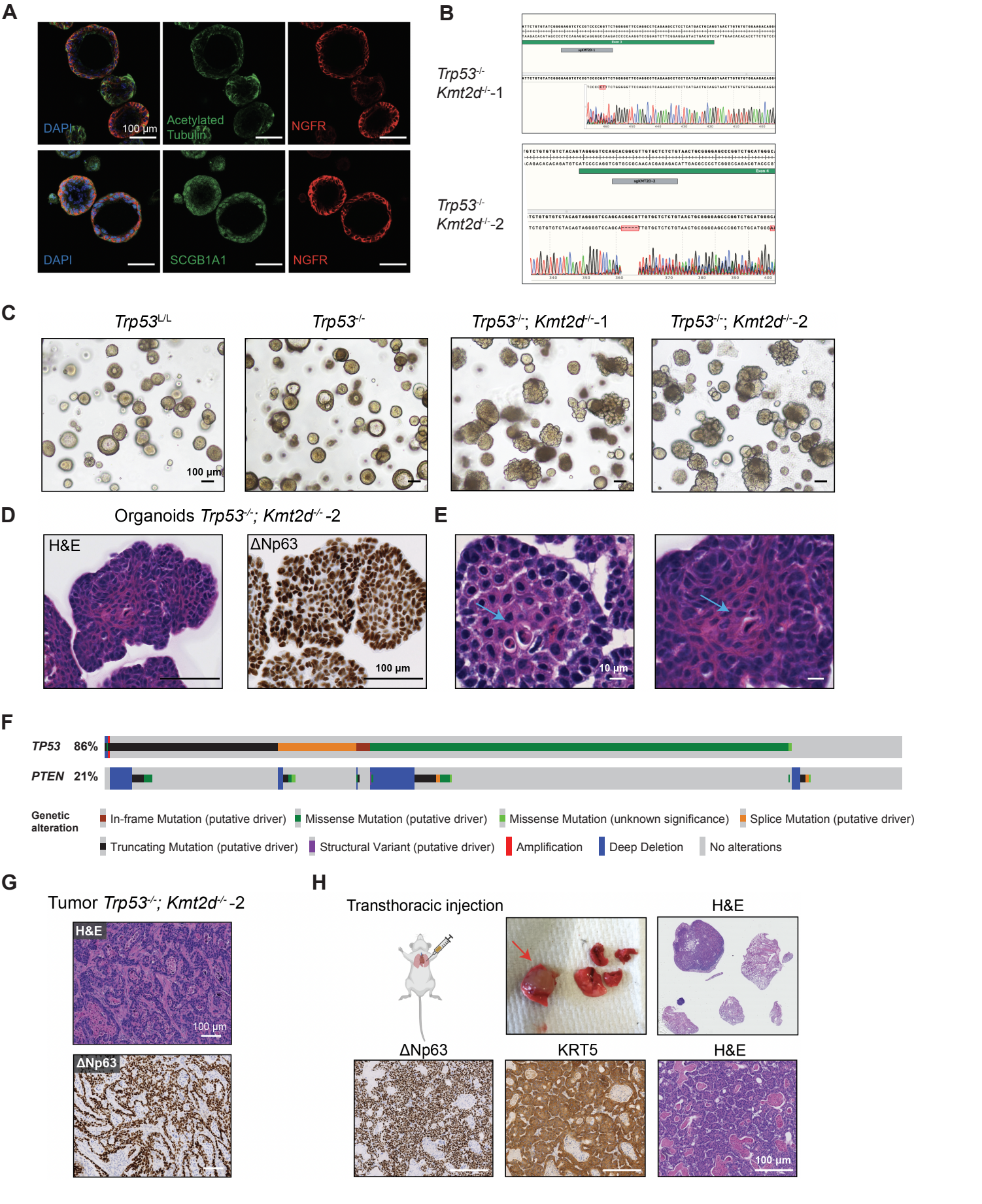
A
DAPI
100 µm
Acetylated Tubulin
NGFR
DAPI
SCGB1A1
NGFR
B
Trp53-/- Kmt2d-/--1
Trp53-/- Kmt2d-/--2
C
Trp53L/L
Trp53-/-
Trp53-/-; Kmt2d-/--1
Trp53-/-; Kmt2d-/--2
100 µm
D
Organoids Trp53-/-; Kmt2d-/- -2
H&E
ΔNp63
100 µm
E
10 µm
F
TP53 86%
PTEN 21%
Genetic alteration
In-frame Mutation (putative driver)
Missense Mutation (putative driver)
Missense Mutation (unknown significance)
Splice Mutation (putative driver)
Truncating Mutation (putative driver)
Structural Variant (putative driver)
Amplification
Deep Deletion
No alterations
G
Tumor Trp53-/-; Kmt2d-/- -2
H&E
100 µm
ΔNp63
H
Transthoracic injection
H&E
ΔNp63
KRT5
H&E
100 µm

Figure S2. *Kmt2d* deletion transforms the lung basal cell organoids to LUSC, related to Figure 1

(A) Representative images of immunofluorescence staining of *Trp53*$^{L/L}$ basal cell organoids after 7 days of culture. Organoids were stained with DAPI (blue), NGFR (red), Acetylated Tubulin (green) and SCGB1A1 (green). NGFR, Acetylated Tubulin and SCGB1A1 mark the basal cells, ciliated cells, and club cells, respectively. Scale bars, 100 μm.

(B) Representative chromatogram sequences of *Kmt2d* loci in the *Trp53*$^{-/-}$; *Kmt2d*$^{-/-}$-1 and *Trp53*$^{-/-}$; *Kmt2d*$^{-/-}$-2 organoids. *Trp53*$^{-/-}$; *Kmt2d*$^{-/-}$-1 and *Trp53*$^{-/-}$; *Kmt2d*$^{-/-}$-2 organoids were generated from 2 different sgRNA targeting *Kmt2d*.

(C) Representative brightfield images of organoids with indicated genotypes after 7 days of culture. *Trp53*$^{-/-}$; *Kmt2d*$^{-/-}$-1 and *Trp53*$^{-/-}$; *Kmt2d*$^{-/-}$-2 organoids were generated from 2 different sgRNA targeting *Kmt2d*. Scale bars, 100 μm.

(D) Representative images of hematoxylin and eosin (H&E) staining and immunohistochemistry (IHC) staining of ΔNp63 in *Trp53*$^{-/-}$; *Kmt2d*$^{-/-}$-2 organoids. Scale bars, 100 μm.

(E) Higher magnification H&E staining images of *Trp53*$^{-/-}$; *Kmt2d*$^{-/-}$ organoids shown in Figure 1E (left) and Figure S2D (Right). The arrows highlight the regions of squamous differentiation. Scale bars, 10 μm.

(F) OncoPrint showing frequency of *PTEN* mutations and their co-occurrence with *TP53* mutations in human LUSC database (TCGA, PanCancer Atlas, n=469).

(G) Representative images of H&E staining and IHC staining of ΔNp63 in tumors devied from *Trp53*$^{-/-}$; *Kmt2d*$^{-/-}$-2 organoids. Scale bars, 100 μm.

(H) Schematic illustration of transthoracic injection of *Trp53*$^{-/-}$; *Kmt2d*$^{-/-}$ organoids and representative images showing tumor-bearing lungs, H&E and IHC staining of ΔNp63 and KRT5 of the orthotopic lung tumors. Scale bars, 100 μm.

Figure S3

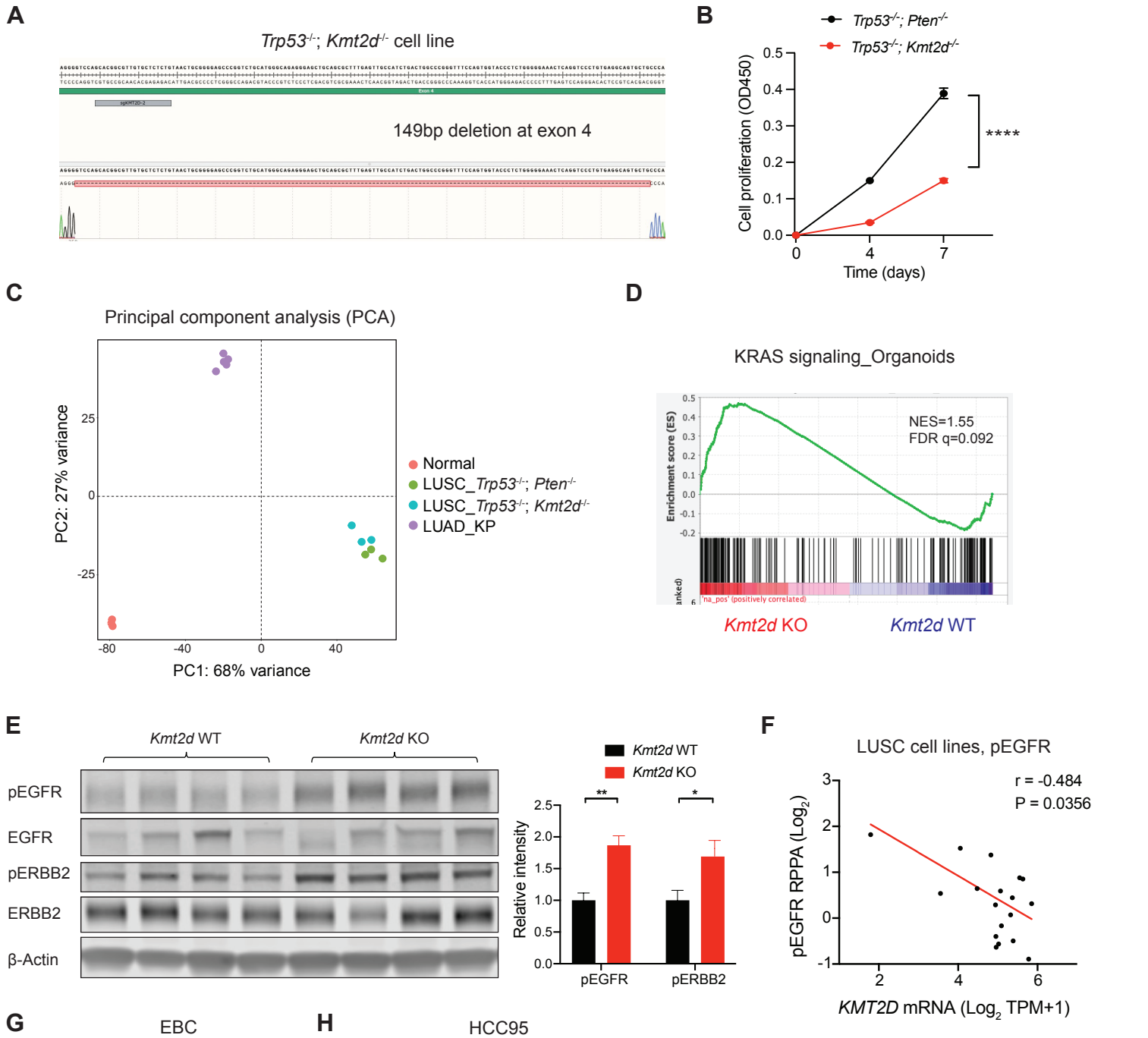
A
Trp53-/-; Kmt2d-/- cell line
149bp deletion at exon 4
B
Trp53-/-; Pten-/-
Trp53-/-; Kmt2d-/-
Cell proliferation (OD450)
Time (days)
****
C
Principal component analysis (PCA)
PC2: 27% variance
PC1: 68% variance
Normal
LUSC_Trp53-/-; Pten-/-
LUSC_Trp53-/-; Kmt2d-/-
LUAD_KP
D
KRAS signaling_Organoids
Enrichment score (ES)
NES=1.55
FDR q=0.092
Kmt2d KO
Kmt2d WT
E
Kmt2d WT
Kmt2d KO
pEGFR
EGFR
pERBB2
ERBB2
β-Actin
Relative intensity
F
LUSC cell lines, pEGFR
r = -0.484
P = 0.0356
pEGFR RPPA (Log2)
KMT2D mRNA (Log2 TPM+1)
G
EBC
sgCtrl
sgKMT2D -1
sgKMT2D -2
pEGFR
EGFR
β-Actin
H
HCC95
sgCtrl
sgKMT2D -1
sgKMT2D -2
pEGFR
EGFR
β-Actin

Figure S3. *Kmt2d* deletion drives LUSC tumorigenesis and activates RTK-RAS signaling, related to Figures 2 and 3

(A) Representative chromatogram sequence of *Kmt2d* locus of the *Trp53*$^{-/-}$; *Kmt2d*$^{-/-}$ cell line.

(B) Proliferation of *Trp53*$^{-/-}$; *Kmt2d*$^{-/-}$ and *Trp53*$^{-/-}$; *Pten*$^{-/-}$ cells *in vitro*. Data shown as means ± SEM. ****p < 0.0001 (ANOVA).

(C) Principal component analysis (PCA) of gene expression in normal mouse lung tissues, LUAD (*Kras*^{G12D}; *Trp53*$^{-/-}$, KP) and LUSC (*Trp53*$^{-/-}$; *Kmt2d*$^{-/-}$ and *Trp53*$^{-/-}$; *Pten*$^{-/-}$).

(D) GSEA analysis showing significantly enriched KRAS signaling comparing *Kmt2d* KO (*Trp53*$^{-/-}$; *Kmt2d*$^{-/-}$) versus *Kmt2d* WT (*Trp53*$^{-/-}$) organoids.

(E) Western blot of pEGFR, EGFR, ERBB2, pERBB2 and β-Actin, and quantification of relative pEGFR and pERBB2 levels in *Kmt2d* KO (*Trp53*$^{-/-}$; *Kmt2d*$^{-/-}$) and *Kmt2d* WT (*Trp53*$^{-/-}$; *Pten*$^{-/-}$) LUSC tumors. Data shown as means ± SEM. *p < 0.05, **p < 0.01 (unpaired two-tailed t test).

(F) Scatterplots showing negative correlation of *KMT2D* mRNA levels with pEGFR in human LUSC cell lines (n=19) from the DepMap dataset (depmap.org/portal/). r, Pearson's correlation coefficient.

(G) Western blot of pEGFR, EGFR, and β-Actin in EBC1-sgCtrl and EBC1-sgKMT2D cells. EBC1-sgKMT2D-1 and EBC1-sgKMT2D-2 cells were generated from 2 different sgRNA targeting *KMT2D*.

(H) Western blot of pEGFR, EGFR, and β-Actin in HCC95-sgCtrl and HCC95-sgKMT2D cells. HCC95-sgKMT2D-1 and HCC95-sgKMT2D-2 cells were generated from 2 different sgRNA targeting *KMT2D*.

Figure S4

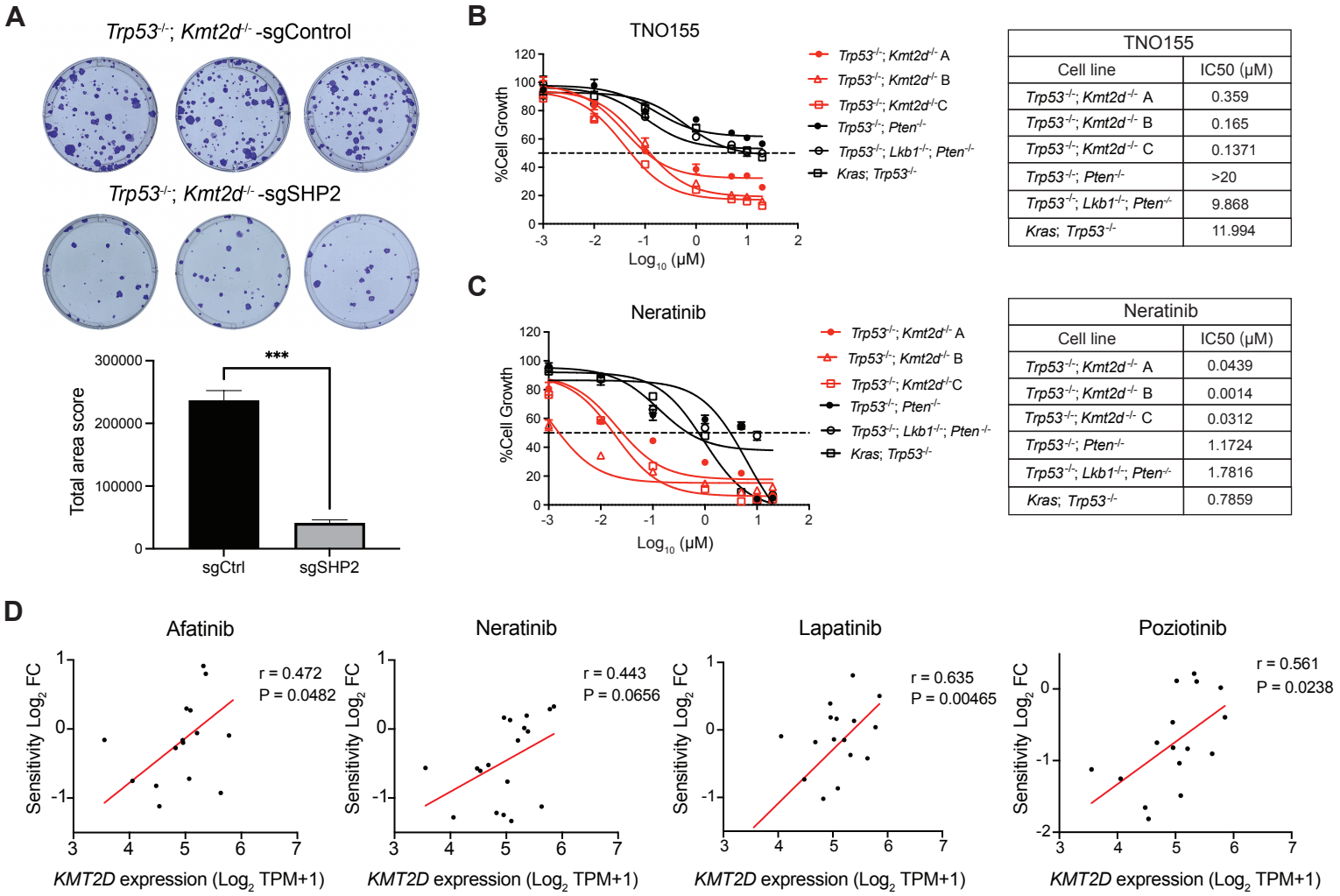

TNO155	
Cell line	IC50 (μM)
Trp53$^{-/-}$; *Kmt2d*$^{-/-}$ A	0.359
Trp53$^{-/-}$; *Kmt2d*$^{-/-}$ B	0.165
Trp53$^{-/-}$; *Kmt2d*$^{-/-}$ C	0.1371
Trp53$^{-/-}$; *Pten*$^{-/-}$	>20
Trp53$^{-/-}$; *Lkb1*$^{-/-}$; *Pten*$^{-/-}$	9.868
Kras; *Trp53*$^{-/-}$	11.994

Neratinib	
Cell line	IC50 (μM)
Trp53$^{-/-}$; *Kmt2d*$^{-/-}$ A	0.0439
Trp53$^{-/-}$; *Kmt2d*$^{-/-}$ B	0.0014
Trp53$^{-/-}$; *Kmt2d*$^{-/-}$ C	0.0312
Trp53$^{-/-}$; *Pten*$^{-/-}$	1.1724
Trp53$^{-/-}$; *Lkb1*$^{-/-}$; *Pten*$^{-/-}$	1.7816
Kras; *Trp53*$^{-/-}$	0.7859

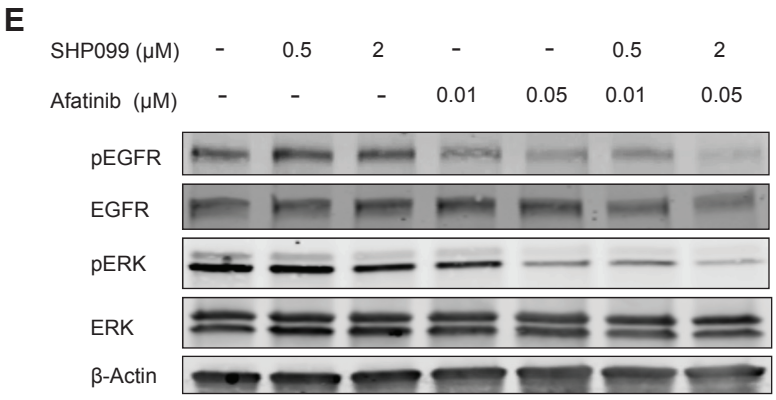

Figure S4. *KMT2D*-deficient LUSC cells are hypersensitive to SHP2 and pan-ERBB inhibition, related to Figure 4

(A) Representative images and quantifications of colony formation assay of *Trp53*$^{-/-}$; *Kmt2d*$^{-/-}$ -sgControl and *Trp53*$^{-/-}$; *Kmt2d*$^{-/-}$ -sgSHP2 cells after 7 days of growth. Data shown as means ± SEM. ***p < 0.001 (unpaired two-tailed t test).

(B and C) Cell viability assays of *Kmt2d* KO LUSC cell lines, *Kmt2d* WT LUSC cell lines, and LUAD (KP) cell line treated with TNO155 (B) and neratinib (C) for 72h. Data presented as mean ± SD (n = 3). The calculated IC50 values of TNO155 and neratinib are shown on the right.

(D) Scatterplots showing correlations of *KMT2D* mRNA levels with sensitivity of afatinib (n=18), neratinib (n=18), lapatinib (n=18), and poziotinib (n=16) (Log2 fold change) in human LUSC cell lines (https://depmap.org/portal/, DepMap drug sensitivity 19Q4 dataset). For the drug sensitivity, lower Log2 FC indicates higher sensitivity. r, Pearson's correlation coefficient.

(E) Western blot of pEGFR, EGFR, pERK, ERK and β-Actin on *Kmt2d* KO (*Trp53*$^{-/-}$; *Kmt2d*$^{-/-}$) LUSC cells treated with SHP099, afatinib alone or in combination for 6h.

Figure S5

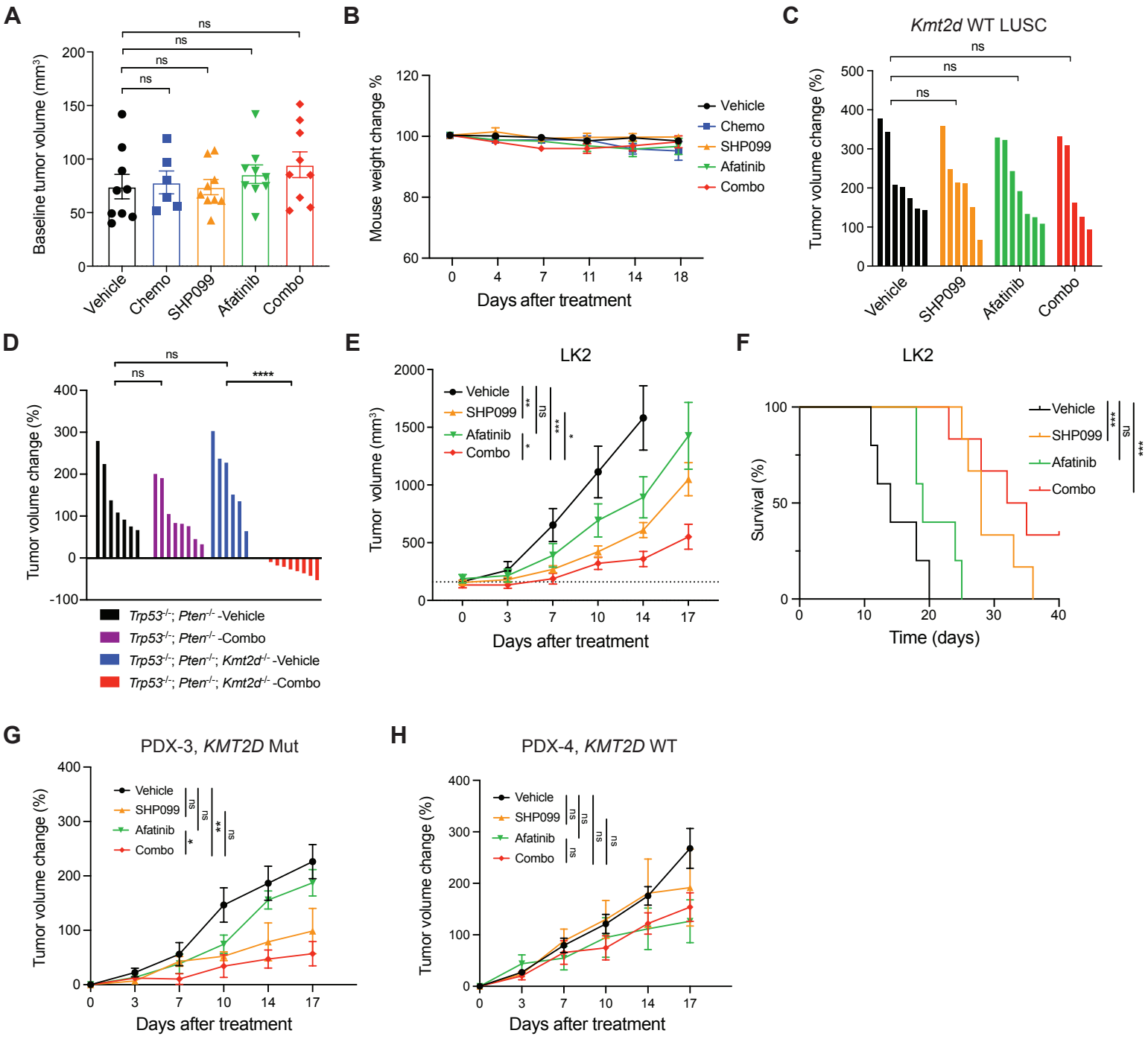
A
Baseline tumor volume (mm3)
ns
Vehicle
Chemo
SHP099
Afatinib
Combo
B
Mouse weight change %
Days after treatment
Vehicle
Chemo
SHP099
Afatinib
Combo
C
Kmt2d WT LUSC
Tumor volume change (%)
D
Tumor volume change (%)
****
Trp53-/-; Pten-/- -Vehicle
Trp53-/-; Pten-/- -Combo
Trp53-/-; Pten-/-; Kmt2d-/- -Vehicle
Trp53-/-; Pten-/-; Kmt2d-/- -Combo
E
LK2
Tumor volume (mm3)
Days after treatment
F
LK2
Survival (%)
Time (days)
G
PDX-3, KMT2D Mut
Tumor volume change (%)
Days after treatment
H
PDX-4, KMT2D WT
Tumor volume change (%)
Days after treatment

Figure S5. SHP099 and afatinib diminish *KMT2D*-deficient LUSC *in vivo,* related to Figure 5

(A) Baseline tumor volumes of *Kmt2d* KO (*Trp53*$^{-/-}$; *Kmt2d*$^{-/-}$) LUSC with indicated treatment. Data shown as means ± SEM. NS, not significant (unpaired two-tailed t test).

(B) Weight changes in mice with indicated treatment. Data shown as means ± SEM.

(C) Waterfall plot of changes in tumor volumes after 2 weeks of treatment in *Kmt2d* WT (*Trp53*$^{-/-}$; *Pten*$^{-/-}$) LUSC. NS, not significant (unpaired two-tailed t test).

(D) Waterfall plot of changes in tumor volumes after 3 weeks of indicated treatment in *Trp53*$^{-/-}$; *Pten*$^{-/-}$ (n=7-8) and *Trp53*$^{-/-}$; *Pten*$^{-/-}$*; Kmt2d*$^{-/-}$ (n=6-8) models. ****p < 0.0001, NS, not significant (unpaired two-tailed t test).

(E) Tumor volume changes of LK2 xenografts following treatments with vehicle (n=9), SHP099 (n=11), afatinib (n=9) alone and in combination (n=11). Data shown as means ± SEM, *p < 0.05, **p < 0.01, ***p < 0.001, NS, not significant (ANOVA).

(F) Kaplan-Meier survival curve for the LK2 LUSC model after indicated treatment. ***p < 0.001, NS, not significant (log-rank test).

(G) Tumor volume changes of *KMT2D* mutant LUSC PDXs (PDX-3) in mice following treatments with vehicle (n=4), SHP099 (n=4), afatinib (n=4) alone and in combination (n=4). Data shown as means ± SEM, *p < 0.05, **p < 0.01, NS, not significant (ANOVA).

(H) Tumor volume changes of *KMT2D* WT LUSC PDXs (PDX-4) in mice following treatments with vehicle (n=4), SHP099 (n=4), afatinib (n=4) alone and in combination (n=4). Data shown as means ± SEM, NS, not significant (ANOVA).

Figure S6

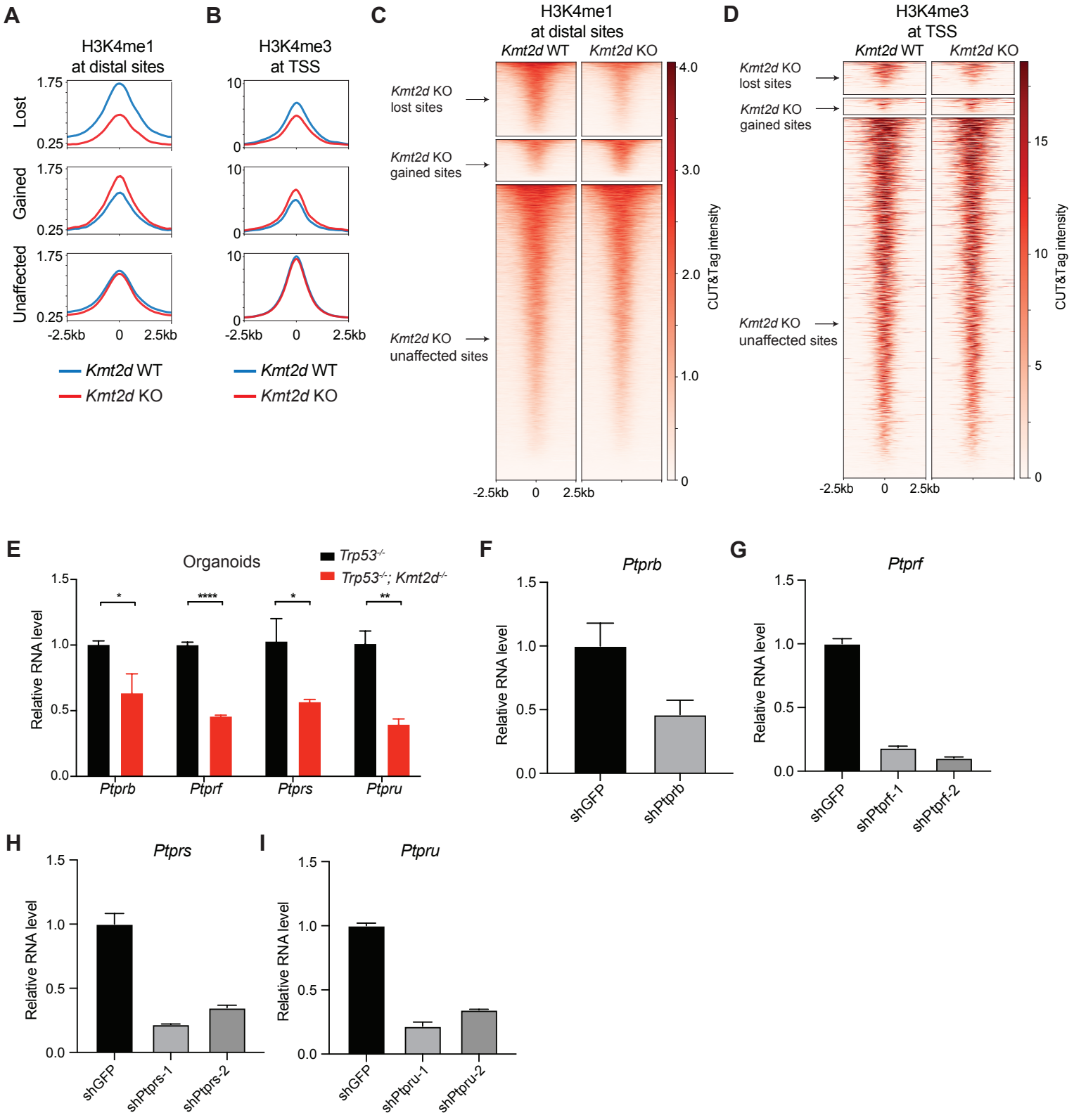
A
H3K4me1
at distal sites
Lost
Gained
Unaffected
1.75
0.25
-2.5kb
0
2.5kb
Kmt2d WT
Kmt2d KO
B
H3K4me3
at TSS
10
0
C
H3K4me1
at distal sites
Kmt2d WT
Kmt2d KO
Kmt2d KO
lost sites
Kmt2d KO
gained sites
Kmt2d KO
unaffected sites
4.0
3.0
2.0
1.0
0
CUT&Tag intensity
D
H3K4me3
at TSS
15
10
5
E
Organoids
Trp53-/-
Trp53-/-; Kmt2d-/-
Relative RNA level
1.5
1.0
0.5
0.0
*
****
*
**
Ptprb
Ptprf
Ptprs
Ptpru
F
Ptprb
shGFP
shPtprb
G
Ptprf
shGFP
shPtprf-1
shPtprf-2
H
Ptprs
shGFP
shPtprs-1
shPtprs-2
I
Ptpru
shGFP
shPtpru-1
shPtpru-2

Figure S6. *Kmt2d* loss reprograms epigenetic landscape and represses expression of protein tyrosine phosphatases in LUSC, related to Figures 6 and 7

(A and B) Averaged CUT&Tag signals of H3K4me1 (A) at distal sites, and H3K4me3 (B) at transcription start sites (TSS), centered at the *Kmt2d* KO-lost, -gained, and -unaffected H3K27ac sites.

(C and D) Heatmaps showing the H3K4me1 (C) at distal sites and H3K4me3 (D) at TSS of CUT&Tag signals in *Kmt2d* WT (*Trp53*$^{-/-}$; *Pten*$^{-/-}$) and *Kmt2d* KO (*Trp53*$^{-/-}$; *Kmt2d*$^{-/-}$) cell lines. Based on the CUT&Tag signal changes, H3K4me1 and H3K4me3 sites were categorized into three groups: *Kmt2d* KO -lost, -gained and -unaffected.

(E) qRT-PCR analysis of *Ptprb*, *Ptprf*, *Ptprs*, and *Ptpru* gene expression in *Trp53*$^{-/-}$ organoids and *Trp53*$^{-/-}$; *Kmt2d*$^{-/-}$ organoids. Data shown as means ± SEM. *p < 0.05, **p < 0.01, ****p < 0.0001 (unpaired two-tailed t test).

(F-I) qRT-PCR analysis of *Ptprb* (F), *Ptprf* (G), *Ptprs* (H) and *Ptpru* (I) gene expression in *Kmt2d* WT (*Trp53*$^{-/-}$; *Pten*$^{-/-}$) cells transfected with shRNA of shPtprb, shPtprf, shPtprs and shPtpru, respectively. Data shown as means ± SEM.